HHS Public Access

Author manuscript

Int J Radiat Oncol Biol Phys. Author manuscript; available in PMC 2021 December 01.

Published in final edited form as:

Int J Radiat Oncol Biol Phys. 2021 December 01; 111(5): 1310–1321. doi:10.1016/j.ijrobp.2021.08.010.

Quantitative Bioluminescence Tomography-guided Conformal Irradiation for Preclinical Radiation Research

Xiangkun Xu, PhD[*,†,a], **Zijian Deng, PhD**[*,†,a], **Hamid Dehghani, PhD**[‡], **Iulian Iordachita, PhD**[§], **Michael Lim, MD**[*,‖], **John W. Wong, PhD**[*], **Ken Kang-Hsin Wang, PhD**[*,†]

[*]Department of Radiation Oncology and Molecular Radiation Sciences, Johns Hopkins University, Baltimore, Maryland

[†]Biomedical Imaging and Radiation Technology Laboratory, Department of Radiation Oncology, University of Texas Southwestern Medical Center, Dallas, Texas

[‡]School of Computer Science, University of Birmingham, Birmingham, West Midlands, United Kingdom

[§]Laboratory for Computational Sensing and Robotics, Johns Hopkins University, Baltimore, Maryland

[‖]Department of Neurosurgery, Stanford University, Stanford, California

Abstract

Purpose: Widely used cone beam computed tomography (CBCT)-guided irradiators in preclinical radiation research are limited to localize soft tissue target because of low imaging contrast. Knowledge of target volume is a fundamental need for radiation therapy (RT). Without such information to guide radiation, normal tissue can be overirradiated, introducing experimental uncertainties. This led us to develop high-contrast quantitative bioluminescence tomography (QBLT) for guidance. The use of a 3-dimensional bioluminescence signal, related to cell viability, for preclinical radiation research is one step toward biology-guided RT.

Methods and Materials: Our QBLT system enables multiprojection and multispectral bioluminescence imaging to maximize input data for the tomographic reconstruction. Accurate quantification of spectrum and dynamic change of in vivo signal were also accounted for the QBLT. A spectral-derivative method was implemented to eliminate the modeling of the light propagation from animal surface to detector. We demonstrated the QBLT capability of guiding conformal RT using a bioluminescent glioblastoma (GBM) model in vivo. A threshold was determined to delineate QBLT reconstructed gross target volume (GTV_{QBLT}), which provides the best overlap between the GTV_{QBLT} and CBCT contrast labeled GBM (GTV), used as the ground truth for GBM volume. To account for the uncertainty of GTV_{QBLT} in target positioning

Corresponding author: Ken Kang-Hsin Wang, PhD; kang-hsin.wang@utsouthwestern.edu.

[a]Xiangkun Xu and Zijian Deng contributed equally to the work.

Research data are stored in an institutional repository and will be shared upon request to the corresponding author.

Supplementary material associated with this article can be found, in the online version, at doi:10.1016/j.ijrobp.2021.08.010.

and volume delineation, a margin was determined and added to the GTV_{QBLT} to form a QBLT planning target volume (PTV_{QBLT}) for guidance.

Results: The QBLT can reconstruct in vivo GBM with localization accuracy within 1 mm. A 0.5-mm margin was determined and added to GTV_{QBLT} to form PTV_{QBLT}, largely improving tumor coverage from 75.0% (0 mm margin) to 97.9% in average, while minimizing normal tissue toxicity. With the goal of prescribed dose 5 Gy covering 95% of PTV_{QBLT}, QBLT-guided 7-field conformal RT can effectively irradiate 99.4 ± 1.0% of GTV.

Conclusions: The QBLT provides a unique opportunity for investigators to use biologic information for target delineation, guiding conformal irradiation, and reducing normal tissue involvement, which is expected to increase reproducibility of scientific discovery.

Introduction

Several groups have initiated efforts to develop small-animal irradiators that mimic clinical radiation therapy (RT).[1–6] The major modality used to guide irradiation is cone beam computed tomography (CBCT).[7–9] However, CBCT is less adept at localizing soft tissue targets growing in a low image contrast environment, further limiting RT studies using important (eg, orthotopic and spontaneous) models. Bioluminescence imaging (BLI) provides strong image contrast; thus, it is an attractive solution for soft tissue targeting, which has been widely used in tracking malignancy and assessing its activity. BLI is commonly acquired at a noncontact imaging geometry,[10–12] based on measurement of emitted surface light from an internal source. However, because optical transport from an internal source is susceptible to irregular animal torso and tissue optical properties, the 2-dimensional BLI is far from being applied to quantify spatial source distributions and to guide focal irradiation.[13,14]

Recognition of these limitations led us to develop 3-dimensional (3D) bioluminescence tomography (BLT) as the image guidance system for small animal irradiator. BLT allows the reconstruction of internal bioluminescent source based on surface BLI.[15–18] Our first BLT was designed to localize the center of mass (CoM) of an optical target for irradiation.[13,19] Spherical volume approximation and CoM proposed in our previous work[19] are a workaround when one does not have actual target volume information for radiation guidance. Knowledge of target volume is a fundamental need for RT. Without such information to guide radiation, large portions of normal tissue can be irradiated unnecessarily, leading to undesired experimental uncertainties. It is imperative that we advance BLT guidance beyond CoM, to a new and precise level of target volume delineation. The recent work conducted by Shi et al[20] is encouraging. They showed the feasibility of applying BLT reconstructed volume to guide irradiation for 4T1 breast carcinoma grown in mouse mammary fat pad and observed the BLT volume decrease after irradiation. However, there is still a large gap between laboratorial development and practical adoption by researchers for their day-to-day biology experiment. To bridge this gap and to translate BLT-guided irradiation for practical use by investigators, we present a comprehensive study of achieving quantitative BLT (QBLT) that enables image-guided conformal irradiation based on 3D bioluminescence distribution in vivo. In this work, different from our and other groups' previous work,[13,19–22] we made great effort not only optimizing hardware,

algorithm, and calibration methods, but also quantifying biologic variation and providing the approach of designing radiation margin for BLT-guided RT.

In BLT, a model of light propagation through tissue to the skin surface is used, in conjunction with an optimization algorithm, to reconstruct the underlying source distribution, which minimizes the difference between calculated and measured surface BL signal. For our workflow, mice were subject to BLI, and later CBCT imaging in our small animal radiation research platform (SARRP), followed by BLI mapped to the animal CBCT image and BLT reconstruction to retrieve target distribution. To apply QBLT as an image-guided system for conformal irradiation in vivo, we have optimized the following aspects. First, a multiprojection and multispectral imaging acquisition was developed to maximize input data information for tomographic reconstruction. Second, the multispectral BLT heavily relies on the accurate quantification of the emission spectrum of bioluminescent cells and dynamic change of in vivo signal. The investigation and corresponding methodology of quantifying the spectrum and in vivo signal are presented. Third, noncontact imaging geometry is commonly adopted in optical tomography, but the challenge of accurately accounting light propagation from tissue surface to optical detector remains. A novel spectral-derivative algorithm, eliminating the free space light propagation error and facilitating target delineation, was proposed recently[18] and first applied to animal study. Fourth, to ensure radiation coverage and to account for QBLT uncertainties in target localization, we have systematically devised target margin in line with clinic practice to enable conformal radiation guidance.

An orthotopic bioluminescent glioblastoma (GBM) model was chosen to demonstrate the QBLT-guided RT, because its low imaging contrast represents a challenging case for CBCT-guided system. We expect that the QBLT-guided small animal irradiators will provide investigators unprecedented capabilities to localize soft tissue target, define target volume for conformal irradiation, and facilitate study reproducibility.

Methods and Materials

System configuration

Our QBLT system was designed as an offline system to maximize the experiment throughput of both SARRP and optical platform, especially when the optical system is only needed for longitudinal study, and radiation-guidance and 3D image are not involved. The QBLT system consists of an optical assembly, a mobile cart, and a transportable mouse bed (Fig. 1a). The assembly is driven by a motorized linear stage to dock onto a mouse bed for imaging. The assembly includes a charge-coupled device (CCD) camera (iKon-L936; Andor Technology, Belfast, United Kingdom) mounted with a 50-mm f/1.2 lens (Nikkor; Nikon, Melville, NY), a filter wheel (Edmund Optics, Barrington, NJ), a 3-mirror system (98% reflective, protected silver coating) and a light-tight enclosure (Fig. 1b). The filter wheel with optical filters is used for multispectral image acquisition to improve BLT reconstruction accuracy.[17,23,24] Four 20-nm FWHM band-pass filters (Chroma Technology, Bellows Falls, VT) at 590, 610, 630, and 650 nm were used. The optical signal emitted from an imaged object was directed to the CCD by the 3-mirror system. Each mirror is oriented 45 degrees relative to optical path (red dashed line, Fig. 1b). The 3-mirror system can rotate 180 degrees

(from −90 to 90 degrees) around imaged object for multiprojection imaging. The image taken at top of the mouse bed is labeled as 0-degree projection imaging. In preparation of imaging session, the imaging chamber was first warmed up with a heat gun (TR89200, 1500W; TR Industrial, Pomona, CA) (Fig. 1a), and the temperature was maintained at 37°C by a resistor loop (Brower Equipment, Houghton, IA) and 7 fans (Digi-Key102-4362-ND; CUI, Tualatin, OR) built inside the chamber. The characterization of the optical system is described in the Appendix E1.

After optical imaging, the mouse bed (Fig. 1c) with animal is transferred from the optical system to SARRP (Xstrahl, Suwanee, GA) for CBCT imaging and irradiation. On the bed, there are 8 imaging markers (PTFE Balls, 2.4 mm diameter; McMaster-Carr, Santa Fe Springs, CA) used for data mapping purpose to register surface BLIs with CBCT image (see Appendix E2. for data mapping detail). The SARRP consists of an x-ray source mounted on a 360-degree rotational gantry, an amorphous silicon flat panel detector, and a 4-dimensional (3-axis translation and 360° rotation) couch. CBCT imaging is acquired by rotating the animal between the x-ray source and detector panel (Fig. 1d). Studied animal was anesthetized and immobilized during the imaging sessions and transport. It was operated within 2 m to the SARRP to minimize the effects of transport on the animal position.[25]

System-specific source spectrum

Because of the multispectral BLT approach, it is important to quantify the system spectral response and the emission spectrum of bioluminescent cells. For simplicity, we used the QBLT system for this measurement, which includes both the system and cell spectral response, and called the resulted spectrum as system-specific source spectrum. Therefore, the wavelength-dependent BLIs can be normalized to the measured spectrum weighting, used as the input data for optical reconstruction. We measured the system-specific spectral weights of GL261-*Luc2* cells at 590, 610, 630, and 650 nm in Petri dishes with cells >80% confluency with concentration of 0.75 mg of D-luciferin (PerkinElmer, Waltham, MA) per 1 mL of phosphate buffer solution. Open-field images without filters were taken before and after each spectral BLI to quantify the in vitro signal variation over time and to eliminate the variation of the in vitro signal as a function of luciferin incubation time. The measured spectrum of the GL261-*Luc2* at 590, 610, 630, and 650 nm at 37°C is 1, 0.916 ± 0.014, 0.674 ± 0.019, and 0.389 ± 0.012 (n = 20), respectively. To assess the spectrum change as function of ambient temperature, we compared 2 conditions 24°C and 37°C representing our BLT system setting without and with the thermosystem turned on, respectively.

Quantify time-resolved in vivo bioluminescence signal

Because in vivo bioluminescence signal can vary over time, and because the change can be animal specific, it is important to quantify the time-resolved in vivo signal for having accurate input data for reconstruction. To build the time-resolved curve for each projection during BLI acquisition, open-field images taken before and after each spectral image along with the time points when the images were taken were used to record the signal variation overtime. A region of interest (ROI) was chosen in the open field image. Because the ROIs in different projections were not from the same physical location of animal surface, the

time-resolved curves between 2 adjacent projections were linked by extrapolating the light intensity from the time-resolved curve of the first projection to the time point when the first open-field image at the second projection was measured. The light intensity recorded from the second projection at this time point was scaled according to the extrapolated light intensity from the first projection. We can therefore combine the time-resolved curves among different projections, quantify the dynamic change of in vivo signal during imaging course, and correct the intensity of each spectral BLI taken at certain time point.

Spectral-derivative method for QBLT reconstruction

For the spectral-derivative method, we used the ratio of the BLIs at adjacent wavelengths as input data for optical reconstruction, as bioluminescence at similar wavelengths encountering a near-identical system response. The mathematical framework can be found in the Appendix E3 or reference.[18] Briefly, the goal of BLT is to solve the BL source distribution or power density, S in Eq. (1) derived from diffusion approximation,[26]

$$G_\lambda w_\lambda S = b_\lambda n \tag{1}$$

where G_λ is a sensitivity matrix for a given wavelength λ related to changes in the measured boundary/surface BLI signal b_λ, G_λ can be constructed from prior knowledge of the optical property of subject, and n is a measurement point specific angular dependent offset to account for the difference between actual surface fluence rate φ_λ and b_λ, and n is assumed to be spectrally invariant, and w_λ is the system-specific spectrum of the light source. By applying logarithm to Eq. (1), and considering the ratio of the data between 2 neighboring wavelengths λ_i and λ_{i+1}, we can write the spectral-derivative form of Eq. (1) as

$$\left[\frac{\log b_{\lambda_i} n}{b_{\lambda_i} n} G_{\lambda_i} w_{\lambda_i} - \frac{\log b_{\lambda_i+1} n}{b_{\lambda_i+1} n} G_{\lambda_i+1} w_{\lambda_i+1}\right] S = \log \frac{b_{\lambda_i}}{b_{\lambda_i+1}} \tag{2}$$

We solved the source distribution S iteratively by applying compressive sensing conjugate gradient optimization algorithm[27] under finite element framework provided by NIRFAST software.[28]

In vivo QBLT validation

To establish the GBM model, GL261-*Luc2* cells were implanted into the left striatum of C57BL/6J mouse (6-8 weeks old, female; The Jackson Laboratory, Bar Harbor, ME) at 3 mm away from burr hole/surgical opening. The GBM-bearing mice, 2 weeks after the implantation, were subject to multispectral and multiprojection BL imaging 10 minutes after D-Luciferin injection. Because the in vivo signal at 590 nm was weak compared with that of other spectral image, which affects the stability of the spectral-derivative method, we chose the images at 610, 630, and 650 nm for QBLT reconstruction for the results presented here. The BLIs were then mapped onto the mesh surface of the imaged mouse generated from the CBCT image. The mapped surface data larger than 10% of the maximum value among all

the surface points were used as input data for QBLT reconstruction. The detail of animal preparation and imaging acquisition and the parameters used in QBLT reconstruction can be found in Appendix E4 and E5, respectively.

Contrast CBCT was used to define the gross target volume (GTV) of GBM bearing mice as the ground truth to validate the accuracy of QBLT target localization. After QBLT imaging session, the mouse was moved to our high-resolution CBCT system[29] for the contrast imaging. The mouse was imaged 1 minute after the contrast injection at dose of 2 gI/kg (Iodixanol, retro-orbital injection 160 μL at 320 mgI/mL; Visipaque, GE Health Care, Chicago, IL). The mouse head region in SARRP CBCT and contrast CBCT image were registered with 3D Slicer (version 4.10.2; https://www.slicer.org/).[30] The GTV was first segmented with 3D Slicer (see Appendix E6) and compared with the GTV reconstructed by QBLT (GTV_{QBLT}). We determined the threshold, based on the maximum value of QBLT reconstructed power density distribution [S, Eq. (1)], best delineating the GTV_{QBLT}, by analyzing the Dice coefficient between GTV_{QBLT} and GTV, as $2(GTV_{QBLT} \cap GTV)/(GTV_{QBLT} + GTV)$.

In vivo QBLT-guided conformal irradiation

A margin accounting for the uncertainty of QBLT target localization (eg, positioning and volume determination) was added to GTV_{QBLT} to form a QBLT planning target volume (PTV_{QBLT}) for radiation guidance. We generated a 7-field conformal radiation plan using an SARRP treatment planning system with the goal of 5 Gy as the prescribed dose to cover 95% of the PTV_{QBLT} and 100% of the GTV_{QBLT}. To confirm the QBLT-guided GBM irradiation qualitatively, we perform the pathologic analysis with immunohistochemical staining (see Appendix E7) to visualize cell nuclei and DNA double-strand breaks using DAPI and γ-H2AX, respectively.

Data distribution and statistical analysis

Nonparametric box plots (MATLAB R2019b; MathWorks, Natick, MA) were used to display distributions of the Dice coefficients as a function of threshold values, tumor and normal tissue coverage as function of PTV_{QBLT} margin size, and dosimetric parameters for single field and QBLT-guided plan comparison. The area between the bottom (25%) and top (75%) of the box edge indicates the degree of data spread. The “black band” within the box represents the 50th percentile, or median number. An outlier is defined as the data falling outside the range of $q_3 + w \times (q_3 - q_1)$ to $q_1 - w \times (q_3 - q_1)$, where w is the maximum whisker length, and q_1 and q_3 are the 25th and 75th percentiles of the sample data, respectively. The MATLAB default value of $w = 1.5$ was used; it renders, at a given normal distribution, the data falling beyond the whisker length corresponds to 0.7% coverage of the data, outside 2.7 standard deviation.

Statistical significance of differences in averages was determined using a 2-tailed paired Student t test (Microsoft Excel 2016; Microsoft, Redmond, WA); $P < .05$ was considered significant.

Results

The effect of ambient temperature and the quantification of interanimal signal variation

Figure 2a shows that in vitro BL intensity of the GL261-*Luc2* cells can increase significantly by 2-fold as the ambient temperature increases from 24°C to 37°C. Beyond maintaining physiologic function, keeping animal at the normal body temperature of 37°C during BL imaging session is also favorable to shorten the image acquisition time, and therefore increase throughput. Figure 2b further illustrates that the system-specific spectrum of the GL261-*Luc2* cells can be red-shifted, when ambient temperature is increased.

Figure 2c shows the time-resolved in vivo BL signal is animal-specific. For each imaged animal, as one can take spectral BLIs at different time points, the animal-specific signal variation could affect the accuracy of the input spectral BL data. We use mouse 3 from Figure 2c as an example; with the method described previously, we can build the animal-specific time-resolved bioluminescence curve over the entire multiprojection imaging course (Fig. 2d). With this curve, we can eliminate the effect of interanimal and physiologic variation on each spectral BLI taken at a certain time point.

In vivo QBLT

To demonstrate the QBLT capability in retrieving target in vivo, GBM-bearing mice were used for BL imaging and reconstruction. Figure 3a shows the BLIs taken at −90, 0, and 90 degrees projection, and then mapped to the mesh surface generated from the mouse CBCT image (Fig. 3b). The corresponding GTV_{QBLT} is qualitatively matched to the GTV (Fig. 3c), if a threshold 0.5 of maximum reconstructed BL power density was applied. We justify the 0.5 threshold as the optimal value for QBLT in target delineation using Dice coefficient (Fig. 3d), with the most overlapped volume between the GTV_{QBLT} and GTV. Furthermore, although there is no significant difference of the Dice coefficient between the threshold 0.5 and 0.6 groups, the variation of the data spread is smaller, and the median value of the Dice coefficient is larger for the 0.5 group than that for the 0.6 group. These reasons support our choice of picking the 0.5 threshold value to delineate the GTV_{QBLT}. As the threshold was continuously increased, GTV_{QBLT} became smaller, and deviated from the GTV, introducing larger data spread as shown in the cases of threshold 0.7-0.8. Moreover, the deviation of CoMs between GTV_{QBLT} and GTV is 0.62 ± 0.16 mm (n = 10). The individual 10 mice result of the GTV_{QBLT} coverage can also be found in Figure E1.

Margin design for PTV_{QBLT}

Although the GTV_{QBLT} qualitatively matches the GTV (Fig. 3c), there is still deviation between the 2 quantities in terms of volume and positioning. To account for these deviations and to ensure irradiation coverage of the tumor volume, we added a uniform margin to GTV_{QBLT} and formed the PTV_{QBLT} for radiation guidance. We investigated optimal margin size by evaluating the GBM volume coverage with conformal index of ($PTV_{QBLT} \cap$ GTV)/GTV and normal tissue coverage with ($PTV_{QBLT} - PTV_{QBLT} \cap GTV)/V_{head}$, where V_{head} is the volume of mouse head (Fig. 4a). Without margin (0 mm expansion), large variation of tumor coverage is expected, average 75.0% varying from 63.6% to 84.7% within 25% to 75% data range and median number at 76.4%. We observed with merely a 0.5-mm

margin expansion, the GTV can be covered by the PTV_{QBLT} at average 97.9% with much smaller variation (97.6%–99.9%) within 25% to 75% data range and median number at 99.2%, compared with the case of 0 mm margin, while the normal tissue inclusion is only at average 1.2%. As we further increased the margin, the benefit of tumor coverage is not statistically significant, but more normal tissue toxicity is introduced. We therefore chose 0.5 mm margin for the studies described later. A representative case is shown in Figure 4b–d to illustrate the PTV margin expanded from reconstructed GTV_{QBLT}. Other individual mice result of margin application can also be found in Figure E1.

In vivo QBLT-guided conformal irradiation

Figure 5a1–a3 shows a representative case of a 7-field noncoplanar beam arrangement to cover the PTV_{QBLT} (Fig. 4b–d). A 5 × 5-mm^2 beam collimator was used, and the CoM of GTV_{QBLT} was set as the beam isocenter (pink points). The corresponding dose distributions are shown in Figure 5b1–b3, where 5 Gy was prescribed to cover 95% of the PTV_{QBLT}. Although we were limited by available collimator size, the QBLT-guided 7-field plan can still effectively cover the PTV_{QBLT} and GTV. For comparison, we generated the dosimetric plan of single beam irradiation (Fig. 5c1–c3), commonly used in radiobiology studies.[31–34] Because of the lack of soft tissue contrast and volumetric information for conventional CBCT-guided system, the common approach for GBM irradiation is setting radiation isocenter at cell implantation location and directing single beam through a surgical burr hole.[31,34] Because no tumor volume information is available, one can only guide the irradiation by the surgical opening at the skull surface indicated in the CBCT. The contrast-labeled GBM (GTV, blue contour in Fig. 5c1–c3) was only used to compare the dosimetric coverage of the GBM volume between the single beam and QBLT-guided 7-beam plan. For a day-to-day biology experiment, the contrast image is not ideal for image guidance using SARRP, which is limited by fast contrast clearance and SARRP CBCT performance. For the single-beam scenario presented in this study, 5 Gy was prescribed to the cell implementation site (yellow dots) 3 mm away from the opening. The single-field plan under-dosed the GTV (red line vs. blue contour) and led to undesired normal tissue irradiation. The dose-volume histogram (Fig. 5d) shows 100% of GTV covered by the 5-Gy prescribed dose with the 7-field conformal plan, and in contrast, only 54% coverage is seen from the single field plan. The GTV_{QBLT} is also 100% covered by the 7-field plan. It is expected that the 7-field plan introduced a larger portion of low-dose bath in a normal tissue region, which is a trade-off for high conformality of target coverage and reduction of the normal tissue toxicity at high dose. From our mice cohort (n = 10), with QBLT-guided conformal irradiation, we can achieve 100% of the prescribed dose covering 99.4 ± 1.0% (capped at 100%) of GTV versus 65.5 ± 18.5% coverage with the single field irradiation. We further compare the target volume coverage for the single-field and QBLT-guided 7-field plan using the metrics of D_{100}, D_{50} and D_2 (Fig. 5e). Taking the D_{100} as an example, it is the deposited dose being able to cover 100% of the GTV. These metrics indicate the dosimetric heterogeneities introduced by a given irradiation technique. The D_{100} boxplot shows that none of the single-field plan can deliver the prescribed dose of 5 Gy covering 100% of GTV, and 40% of the animals did not even reach D_{100} at 4 Gy. The large box size and extensive D_{100} variation (0.1-4.9 Gy) renders large experimental uncertainty. In contrast, for QBLT-guided 7-field irradiation, D_{100} of GTV only vary from 4.9 to 5.5 Gy within 25% to 75% data range,

with a minimum 4.5 Gy, maximum 6.2 Gy, and median value at 5.2 Gy, which indicates superior tumor coverage and smaller dose variation. Larger D_{50} and D_2 are expected in the case of both 7-field GTV and GTV_{QBLT}, compared with the single-field group, because of the prescribed dose aimed to cover PTV_{QBLT}, leading to a larger hot region inside the GTV and GTV_{QBLT}. We further compared the D_{100}, D_{50} and D_2 between the GTV and GTV_{QBLT} group, and there is no significant difference between these metrics. This result suggests that one could use GTV_{QBLT} to evaluate the dosimetric coverage of GTV.

Because of the limitation of pathologic staining, we used 2 mice to demonstrate the 3D feature of the QBLT-guided conformal irradiation (Fig. 6). The high-dense DNA region/GBM location shown in the DAPI images (Fig. 6a1–a2) is overlapped well with the irradiated area stained by the γ-H2AX (Fig. 6b1–b2, 6c1–c2). These results confirm that QBLT can guide SARRP to effectively irradiate the GBM. It is worth noting that γ-H2AX staining is highly sensitive to radiation, and it is challenging to determine the exact threshold dose inducing the DNA double-strand breaks. We did not use γ-H2AX staining as quantitative measure, but a qualitative method to confirm the GBM irradiation. In fact, even the dose outside GBM is low, and γ-H2AX can still reveal one of the radiation beam passage (Fig. 6b2).

Discussion

CBCT-guided irradiation[1,2,4,6] provides guidance capability, but it is limited to localized soft tissue targets. Although one might consider contrast imaging for target delineation, because of fast clearance and the use being limited to well-vascularized tumor models, it is not an ideal modality to guide irradiation. BLI thus offers an attractive solution; however, the intensity and distribution of commonly used techniques are nonlinearly dependent on the spatial location of internal source, tissue optical properties, and animal shape.[35] Thus, the spatial distribution of bioluminescent tumor is not accessible for quantitation with BLI. It is imperative to develop the QBLT to accurately quantify the spatial distribution of the underlying tumor for radiation guidance. Several recent studies have shown the potential of applying BLT for radiation guidance.[13,19–22] The significance of this work is that we devised a comprehensive approach to systematically tackle the known challenging of optical tomography for in vivo target delineation, quantify its uncertainties in both biology and tissue optics for localization, and present the practicality for radiation guidance. Through this work, we expect to increase the recognition of BLT and its adoption for biology-guided irradiation.

Considering the underdetermined nature of BLT, we chose the multiprojection and multispectral imaging acquisition to maximize input information for QBLT reconstruction.[17,23] Accurate target reconstruction depends on whether we have correct surface images as input. Ambient temperature does not just affect imaging acquisition time or experiment throughput; it also affects the accuracy of the multispectral BLT reconstruction, which is closely related to the BL spectrum (Fig. 2a–b). The in vitro cell spectrum is part of our input information for the multispectral BLT reconstruction. Therefore, it is necessary to maintain a consistent ambient temperature (preferably 37°C) equal to the temperature of a normal mouse body, between the in vitro spectrum

measurement and in vivo bioluminescence imaging acquisition. We also presented that the kinetics of in vivo luciferin uptake is animal specific (Fig. 2c–d), which can affect the amplitude of the surface spectral data taken at different time points and potentially lead to erroneous BLT target localization. Furthermore, in noncontact imaging geometry, one major challenge is accounting for the light propagation from the skin to the optical detector. Existing approaches typically use a model of the imaging system that is usually computationally intensive or of limited accuracy.[36,37] As the BLIs at adjacent wavelengths encounter a near-identical system response, the spectral-derivative method[18] eliminates the need for complicated system modeling. With our comprehensive approaches, we demonstrate that QBLT is able to define approximated GBM volume in vivo with the localization accuracy <1 mm.

The distribution of the BLT-reconstructed volume depends on the choice of threshold, which determines the accuracy of radiation guidance. There are various threshold values used in optical tomography studies.[38–40] The challenge of threshold selection in BLT is finding the value best representing actual target volume throughout study animals. We derived the strategy that determines the optimal threshold value 0.5 using the Dice coefficient (Fig. 3d). Although the optimal threshold provides encouraging result of delineating the GBM volume (Fig. 3c), the QBLT-reconstructed volume is inevitably suffered from the resolution limitation and multiple scattering nature of diffuse optical tomography where actual tumor shape delineation is challenging. We innovated designing a margin to account for the uncertainties of QBLT in target localization. Without margin, a large variation of tumor coverage is expected, which translates to large experimental uncertainties. In contrast, after adding a 0.5-mm margin, the averaged tumor coverage was largely improved from 75.0% to 97.9%, and the variation was significantly reduced (Fig. 4a). The PTV_{QBLT} was designed to account for the localization uncertainties of the GTV_{QBLT} in target positioning and volume delineation. Regarding the potential positioning error caused by animal transport, from our study,[25] as long as animals are anesthetized with effective immobilization during transport and the off-line optical system is in close proximity (< 5 m) to SARRP, the positioning error can be maintained within 0.2 mm. Most importantly, when we mapped the 2-dimensional bioluminescence images to the surface of 3D mesh generated from SARRP CBCT image, this positioning error, if any, will be propagated to the data mapping and finally to the BLT reconstruction, which had been accounted in PTV_{QBLT}. The SARRP irradiation uncertainty and the image registration uncertainty between SARRP CBCT imaging and our in-house contrast CBCT imaging could be considered further. However, published results have shown that SARRP can deliver the radiation dose at 0.2-mm accuracy.[41] The uncertainty of image registration between SARRP CBCT and our in-house contrast CBCT for mouse brain is within 0.25 mm at the image pixel limit. By adding these uncertainties into our 0.5-mm margin using root sum–squared method, the overall margin would be 0.59 mm, not significantly larger than the 0.5 mm margin. This finding suggests that the major uncertainty for target localization is contributed from the BLT reconstructed volume, GTV_{QBLT}. Moreover, our immunohistochemical staining results have qualitatively validated that PTV_{QBLT} can guide SARRP to effectively irradiate the GBM (Fig. 6). Thus, the PTV_{QBLT} derived in our study is a reasonable estimation to provide sufficient GBM coverage for the QBLT-guided RT. Nevertheless, researchers who are interested in using the

QBLT-guided RT can follow our approach and further optimize the margin size for target coverage based on their research purposes, and irradiator-specific localization errors.

The margin is critical in that it does not only reduce the variation of target coverage but also provides a practical radiation planning volume to make conformal RT possible. It is significant that now we can mimic clinical RT in an orthotopic model to reduce normal tissue involvement and align in vivo experiments with clinical practice. From Figures 5b1–b3, versus 5c1–c3, and 5d, the optical-guided conformal irradiation is far superior than the traditional single field irradiation which can miss target and may lead to wrong experiment conclusions owing to large variation of tumor coverage (Fig. 5e). The similar D_{100}, D_{50}, and D_2 between the GTV and GTV_{QBLT} coverage further validate that with the PTV_{QBLT} derived by proper threshold and margin selection, we can perform high-contrast, optical image–guided irradiation. Our current treatment plan is limited by available collimator size from the commercial SARRP and forward treatment plan scheme. We designed the 7-field conformal plan (Fig. 5a1–a3) with empirically selected gantry and couch positions. In a clinical setting, one would use a multileaf collimator combined with inverse planning to design optimal collimator opening and beam orientation to provide conformal dose coverage. However, preclinical radiation research technology is still behind that of clinical RT, and the advance techniques are underdeveloped.[42–44] With these technologies, one would expect that the dose conformality (Fig. 5b1–b3, 5e) can be improved.

It is worth mentioning that QBLT-guided RT is not limited by the brain tumor model presented in this work. Our preliminary result of applying QBLT-guided conformal irradiation for an orthotopic pancreatic tumor model demonstrated 1.2-mm localization accuracy with 95% PTV_{QBLT} coverage at the prescribed dose (Appendix E8 and Fig. E3). However, guiding irradiation for abdominal tumor is not trivial, because it involves organ movement and strong optical tissue heterogeneities. Further investigation of applying QBLT-guided irradiation for abdominal tumor is ongoing.

This work is significant advance of our previously published BLT-guided CoM irradiation.[19] Because of technology constraints, we were able to provide only the CoM location of a bioluminescent target, and we had to estimate tumor volume by equivalent sphere, established from a tumor growth curve.[19] The spherical volume is designed to be conservative to not miss the target. Despite providing good tumor coverage, it inevitably includes large normal tissue region as discussed previously.[19] With all the developments described here, we could leap toward the quantitative biology-guided irradiation from the geometric-guided scheme (CoM point and equivalent sphere). With QBLT, one does not need to know the tumor growth information to estimate volume, which can be challenging for orthotopic and spontaneous model. The QBLT-guided irradiation is one step closer to a clinical scenario that we can tailor radiation to the reconstructed bioluminescence volume and reduce normal tissue toxicity. Using 2-week-old in vivo GBM as an example, our data shows the volume of normal tissue involvement within PTV_{QBLT} (36.2 ± 9.8 mm^3) derived from the QBLT is half of that (77.6 ± 4.7 mm^3) from the estimated sphere method.[19]

BLI has served as common surrogate to inform tumor activity. One can potentially use the QBLT-reconstructed volume and its BL power to quantify tumor viability in response

to therapeutic intervention. The analogy can be found in positron emission tomography–guided irradiation for radiation planning and tumor response evaluation.[45,46] The QBLT thus complements CBCT-guided irradiators by providing researchers new capabilities for defining target volume for conformal RT, and noninvasively quantifying treatment outcome.

Conclusion

We have enabled quantitative BLT-guided irradiation by optimizing the hardware, algorithm, and calibration method and by addressing the uncertainties introduced by biology and tissue optics in target localization and volume delineation. Our QBLT platform will enhance preclinical RT research with the capabilities of functional targeting beyond anatomic imaging.

Supplementary Material

Refer to Web version on PubMed Central for supplementary material.

Disclosures:

This work was supported by Xstrahl and grants from the National Cancer Institute, National Institutes of Health of USA (R21CA223403, R37CA230341, R01CA240811, and P30 CA006973) and Cancer Prevention and Research Institute of Texas (RR200042).

I.I. receives royalties from Xstrahl and reports grants from the National Institutes of Health, during the conduct of the study; and receives personal fees from Gulmay Medical and Xstrahl, outside the submitted work. In addition, I.I. has a patent issued (“Optical Imaging System and Method of Making and Using the Same”). M.L. reports research support from Arbor, BMS, Accuray, Tocagen, Biohaven, Kyrin-Kyowa and Urogen; is a consultant for Tocagen, SQZ Technologies, VBI, InCephalo Therapeutics, Pyramid Bio, Merck, BMS, Insightec, Biohaven, Sanianoia, Hemispherian, Black Diamond Therapeutics and Novocure; is a shareholder of Egret Therapeutics; retains patents on combination of focused radiation and checkpoint inhibitors, combination of local chemothrapy and checkpoint inhibitors, and checkpoints for Neuro-Inflammation; and provides nonresearch consultancy for Stryker.

I.I. receives royalties from Xstrahl and reports grants from the National Institutes of Health, during the conduct of the study; and receives personal fees from Gulmay Medical and Xstrahl, outside the submitted work. In addition, I.I. has a patent issued (“Optical Imaging System and Method of Making and Using the Same”). M.L. reports research support from Arbor, BMS, Accuray, Tocagen, Biohaven, Kyrin-Kyowa and Urogen; is a consultant for Tocagen, SQZ Technologies, VBI, InCephalo Therapeutics, Pyramid Bio, Merck, BMS, Insightec, Biohaven, Sanianoia, Hemispherian, Black Diamond Therapeutics and Novocure; is a shareholder of Egret Therapeutics; retains patents on combination of focused radiation and checkpoint inhibitors, combination of local chemothrapy and checkpoint inhibitors, and checkpoints for Neuro-Inflammation; and provides nonresearch consultancy for Stryker.

References

1. Wong J, Armour E, Kazanzides P, et al. High-resolution, small animal radiation research platform with x-ray tomographic guidance capabilities. Int J Radiat Oncol Biol Phys 2008;71:1591–1599. [PubMed: 18640502]
2. Clarkson R, Lindsay PE, Ansell S, et al. Characterization of image quality and image-guidance performance of a preclinical microirradiator. Med Phys 2011;38:845–856. [PubMed: 21452722]
3. Pidikiti R, Stojadinovic S, Speiser M, et al. Dosimetric characterization of an image-guided stereotactic small animal irradiator. Phys Med Biol 2011;56:2585–2599. [PubMed: 21444969]
4. Verhaegen F, Granton P, Tryggestad E. Small animal radiotherapy research platforms. Phys Med Biol 2011;56:R55–R83. [PubMed: 21617291]

5. Graves EE, Zhou H, Chatterjee R, et al. Design and evaluation of a variable aperture collimator for conformal radiotherapy of small animals using a microCT scanner. Med Phys 2007;34:4359–4367. [PubMed: 18072501]
6. Sha H, Udayakumar TS, Johnson PB, et al. An image guided small animal stereotactic radiotherapy system. Oncotarget 2016;7:18825–18836. [PubMed: 26958942]
7. Ford EC, Achanta P, Purger D, et al. Localized CT-guided irradiation inhibits neurogenesis in specific regions of the adult mouse brain. Radiat Res 2011;175:774–783. [PubMed: 21449714]
8. Baumann BC, Benci JL, Santoiemma PP, et al. An integrated method for reproducible and accurate image-guided stereotactic cranial irradiation of brain tumors using the small animal radiation research platform. Transl Oncol 2012;5:230–237. [PubMed: 22937174]
9. Redmond KJ, Achanta P, Grossman SA, et al. A radiotherapy technique to limit dose to neural progenitor cell niches without compromising tumor coverage. J Neurooncol 2011;104:579–587. [PubMed: 21327710]
10. Zinn KR, Chaudhuri TR, Szafran AA, et al. Noninvasive bioluminescence imaging in small animals. ILAR J 2008;49:103–115. [PubMed: 18172337]
11. Badr CE, Tannous BA. Bioluminescence imaging: Progress and applications. Trends Biotechnol 2011;29:624–633. [PubMed: 21788092]
12. Mezzanotte L, van 't Root M, Karatas H, et al. In vivo molecular bioluminescence imaging: new tools and applications. Trends Biotechnol 2017;35:640–652. [PubMed: 28501458]
13. Zhang B, Wang KK-H, Yu J, et al. Bioluminescence tomography-guided radiation therapy for preclinical research. Int J Radiat Oncol Biol Phys 2016;94:1144–1153. [PubMed: 26876954]
14. Yu J, Zhang B, Iordachita II, et al. Systematic study of target localization for bioluminescence tomography guided radiation therapy. Med Phys 2016;43:2619–2629. [PubMed: 27147371]
15. Ntziachristos V, Ripoll J, Wang LV, et al. Looking and listening to light: The evolution of whole-body photonic imaging. Nat Biotechnol 2005;23:313–320. [PubMed: 15765087]
16. Wang G, Cong W, Durairaj K, et al. In vivo mouse studies with bioluminescence tomography. Opt Express 2006;14:7801–7809. [PubMed: 19529149]
17. Kuo C, Coquoz O, Troy TL, et al. Three-dimensional reconstruction of in vivo bioluminescent sources based on multispectral imaging. J Biomed Opt 2007;12: 024007. [PubMed: 17477722]
18. Dehghani H, Guggenheim JA, Taylor SL, et al. Quantitative bioluminescence tomography using spectral derivative data. Biomed Opt Express 2016;9:4163–4174.
19. Deng Z, Xu X, Garzon-Muvdi T, et al. In vivo bioluminescence tomography center of mass-guided conformal irradiation. Int J Radiat Oncol Biol Phys 2020;106:612–620. [PubMed: 31738948]
20. Shi J, Udayakumar TS, Xu K, et al. Bioluminescence tomography guided small-animal radiation therapy and tumor response assessment. Int J Radiat Oncol Biol Phys 2018;102:848–857. [PubMed: 29534897]
21. Shi J, Udayakumar TS, Wang Z, et al. Optical molecular imaging-guided radiation therapy part 1: integrated x-ray and bioluminescence tomography. Med Phys 2017;44:4786–4794. [PubMed: 28627007]
22. Shi J, Xu K, Keyvanloo A, et al. A multimodality image guided precision radiation research platform: integrating X-ray, bioluminescence, and fluorescence tomography with radiation therapy. Int J Radiat Oncol Biol Phys 2020;108:1063–1072. [PubMed: 32585336]
23. Cong AX, Wang G. Multispectral bioluminescence tomography: Methodology and simulation. Int J Biomed Imaging 2006;2006:57614. [PubMed: 23165040]
24. Dehghani H, Davis SC, Jiang S, et al. Spectrally resolved bioluminescence optical tomography. Opt Lett 2006;31:365–367. [PubMed: 16480210]
25. Zhang B, Wong JW, Iordachita II, et al. Evaluation of on- and off-line bioluminescence tomography system for focal irradiation guidance. Radiat Res 2016;186:592–601. [PubMed: 27869556]
26. Wang LV, Wu HI. Radiative transfer equation and diffusion theory. Biomedical optics: Principles and imaging. 2009Hoboken, NJ: Wiley; 2009:83–118. 10.1002/9780470177013.ch5 Available at.

27. Basevi HR, Tichauer KM, Leblond F, et al. Compressive sensing based reconstruction in bioluminescence tomography improves image resolution and robustness to noise. Biomed Opt Express 2012;3:2131–2141. [PubMed: 23024907]
28. Dehghani H, Eames ME, Yalavarthy PK, et al. Near infrared optical tomography using NIRFAST: algorithm for numerical model and image reconstruction. Commun Numer Methods Eng 2008;25:711–732. [PubMed: 20182646]
29. Yang Y, Wang KK-H, Eslami S, et al. Systematic calibration of an integrated x-ray and optical tomography system for preclinical radiation research. Med Phys 2015;42:1710–1720. [PubMed: 25832060]
30. Fedorov A, Beichel R, Kalpathy-Cramer J, et al. 3D Slicer as an image computing platform for the quantitative imaging network. Magn Reson Imaging 2012;30:1323–1341. [PubMed: 22770690]
31. Zeng J, See AP, Phallen J, et al. Anti-PD-1 blockade and stereotactic radiation produce long-term survival in mice with intracranial gliomas. Int J Radiat Oncol Biol Phys 2013;86:343–349. [PubMed: 23462419]
32. Zarghami N, Murrell DH, Jensen MD, et al. Half brain irradiation in a murine model of breast cancer brain metastasis: magnetic resonance imaging and histological assessments of dose-response. Radiat Oncol 2018;13:104. [PubMed: 29859114]
33. Gunderson AJ, Yamazaki T, McCarty K, et al. Blockade of fibroblast activation protein in combination with radiation treatment in murine models of pancreatic adenocarcinoma. PLoS One 2019;14:e0211117. [PubMed: 30726287]
34. Andreou T, Williams J, Brownlie RJ, et al. Hematopoietic stem cell gene therapy targeting TGFβ enhances the efficacy of irradiation therapy in a preclinical glioblastoma model. J Immunother Cancer 2021;9:e001143. [PubMed: 33707311]
35. Klose AD, Paragas N. Automated quantification of bioluminescence images. Nat Commun 2018;9:4262. [PubMed: 30323260]
36. Chen X, Gao X, Qu X, et al. Generalized free-space diffuse photon transport model based on the influence analysis of a camera lens diaphragm. Appl Opt 2010;49:5654–5664. [PubMed: 20935713]
37. Guggenheim JA, Basevi HR, Styles IB, et al. Quantitative surface radiance mapping using multiview images of light-emitting turbid media. J Opt Soc Am A 2013;30:2572–2584.
38. Zilberman Y, Kallai I, Gafni Y, et al. Fluorescence molecular tomography enables in vivo visualization and quantification of nonunion fracture repair induced by genetically engineered mesenchymal stem cells. J Orthop Res 2008;26:522–530. [PubMed: 17985393]
39. Ntziachristos V, Schellenberger EA, Ripoll J, et al. Visualization of antitumor treatment by means of fluorescence molecular tomography with an annexin V-Cy5.5 conjugate. Proc Natl Acad Sci USA 2004;101:12294–12299. [PubMed: 15304657]
40. Zacharakis G, Kambara H, Shih H, et al. Volumetric tomography of fluorescent proteins through small animals in vivo. Proc Natl Acad Sci USA 2005;102:18252–18257. [PubMed: 16344470]
41. Matinfar M, Ford E, Iordachita II, et al. Image-guided small animal radiation research platform: Calibration of treatment beam alignment. Phys Med Biol 2009;54:891–905. [PubMed: 19141881]
42. Woods K, Nguyen D, Neph R, et al. A sparse orthogonal collimator for small animal intensity-modulated radiation therapy part I: Planning system development and commissioning. Med Phys 2019;46:5703–5713. [PubMed: 31621920]
43. Woods K, Neph R, Nguyen D, et al. A sparse orthogonal collimator for small animal intensity-modulated radiation therapy. Part II: hardware development and commissioning. Med Phys 2019;46:5733–5747. [PubMed: 31621091]
44. Balvert M, van Hoof SJ, Granton PV, et al. A framework for inverse planning of beam-on times for 3D small animal radiotherapy using interactive multi-objective optimisation. Phys Med Biol 2015;60:5681–5698. [PubMed: 26147184]
45. Guha C, Alfieri A, Blaufox MD, et al. Tumor biology-guided radiotherapy treatment planning: gross tumor volume versus functional tumor volume. Semin Nucl Med 2008;38:105–113. [PubMed: 18243845]
46. Parodi K Vision 20/20: Positron emission tomography in radiation therapy planning, delivery, and monitoring. Med Phys 2015;42:7153–7168. [PubMed: 26632070]

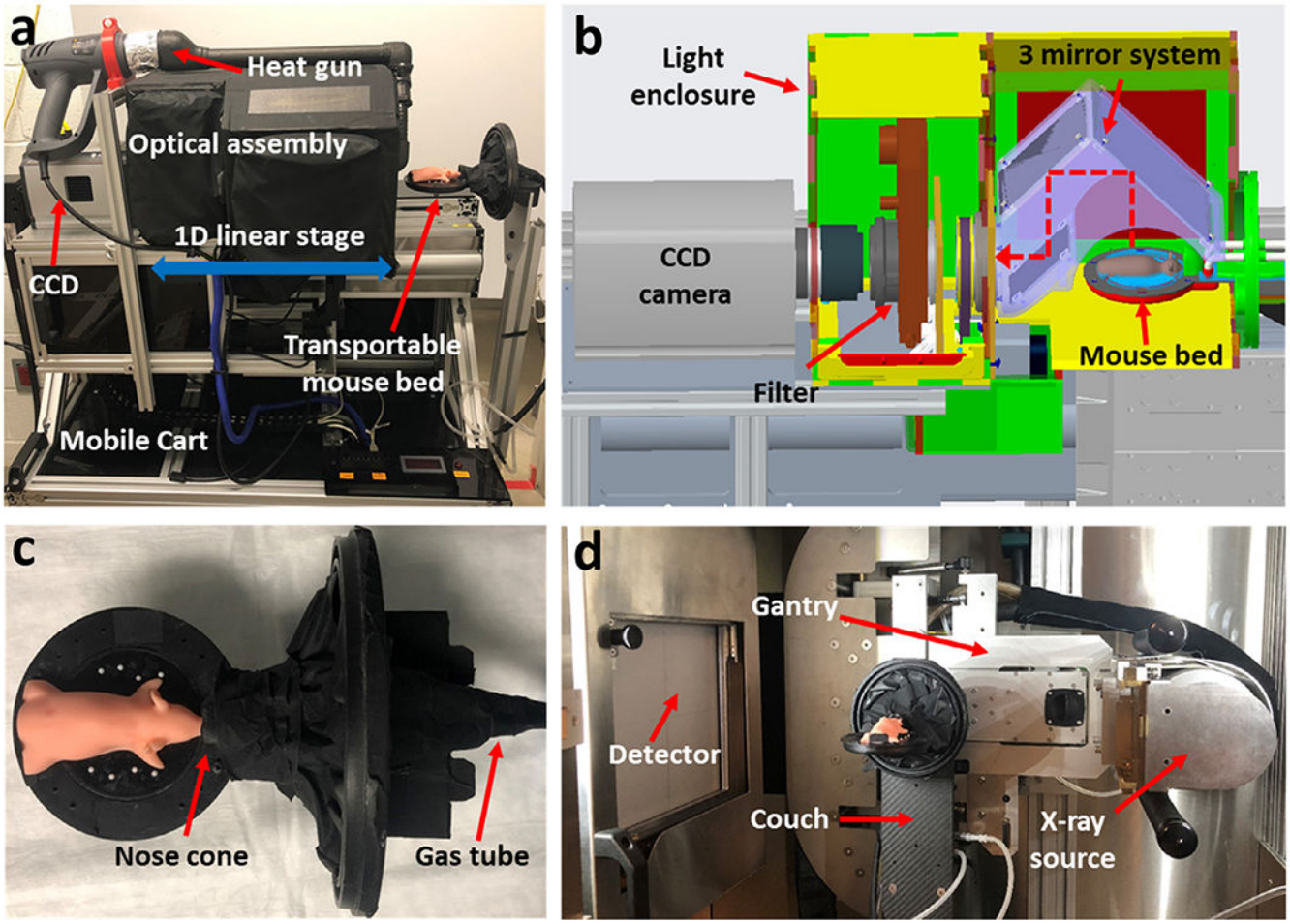

Fig. 1.

(a, b) System configuration for the quantitative bioluminescence tomography. The 3-mirror system attached to the enclosure can rotate and reflect light from object to charge-coupled device. (c) Transportable mouse bed with imaging markers (white plastic balls); the nose cone and gas tube are used to deliver anesthetic gas. (d) Small animal radiation research platform configuration for cone beam computed tomography acquisition. CCD = charge-coupled device.

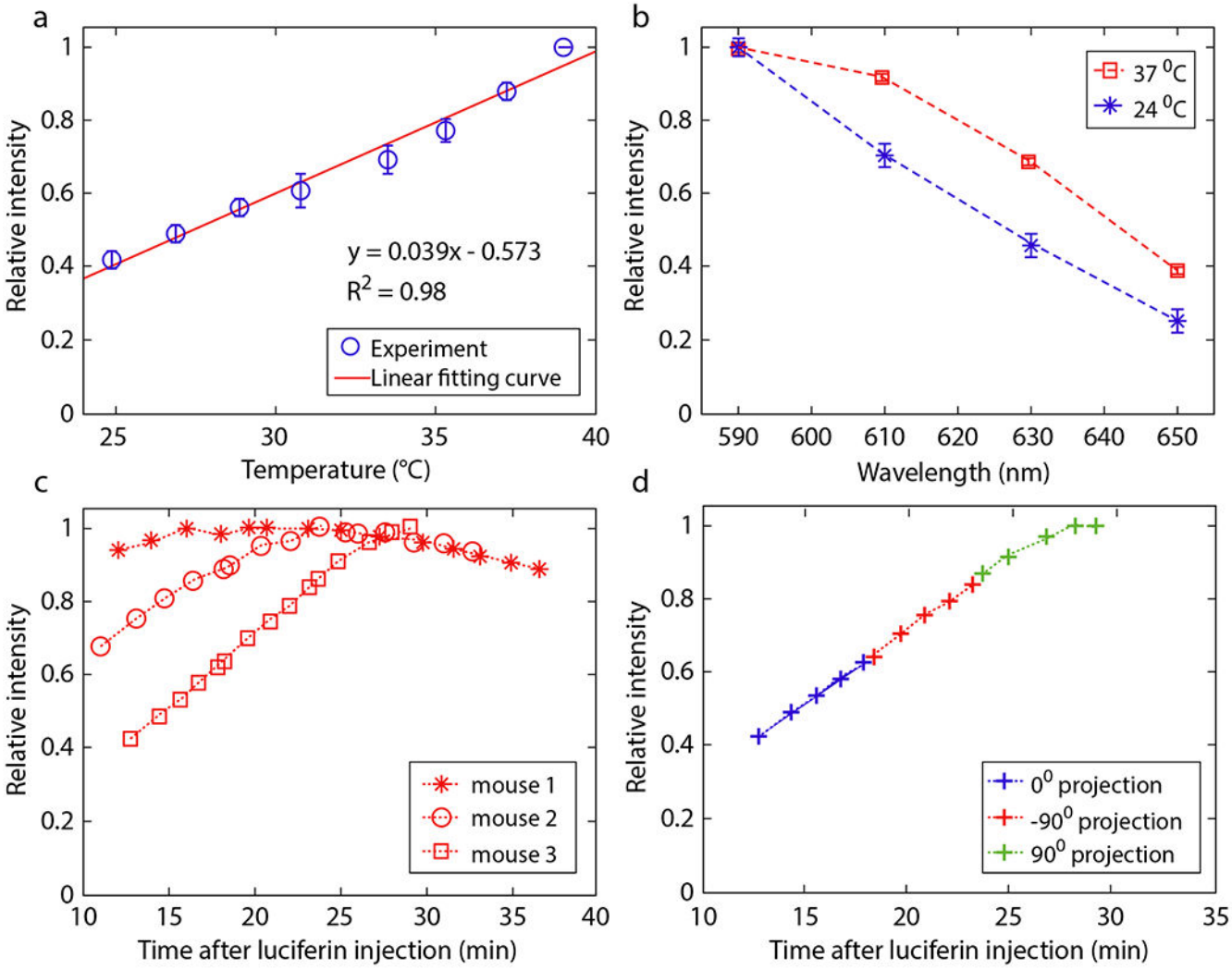

Fig. 2.

Temperature effect on bioluminescence signal in vitro and quantification of interanimal signal variation. (a) In vitro light intensity of GL261-*Luc2* cells versus ambient temperature (n = 5). (b) System-specific spectrum of GL261-*Luc2* for 24°C (n = 6) and 37°C (n = 20). Error bars represent standard deviation. (c) Dynamic change of in vivo bioluminescence signal for 3 glioblastoma-bearing mice, normalized to maximum intensity. (d) Mouse 3 from (c) is used to illustrate the formation of the overall time-resolved curve combined from 3 projections.

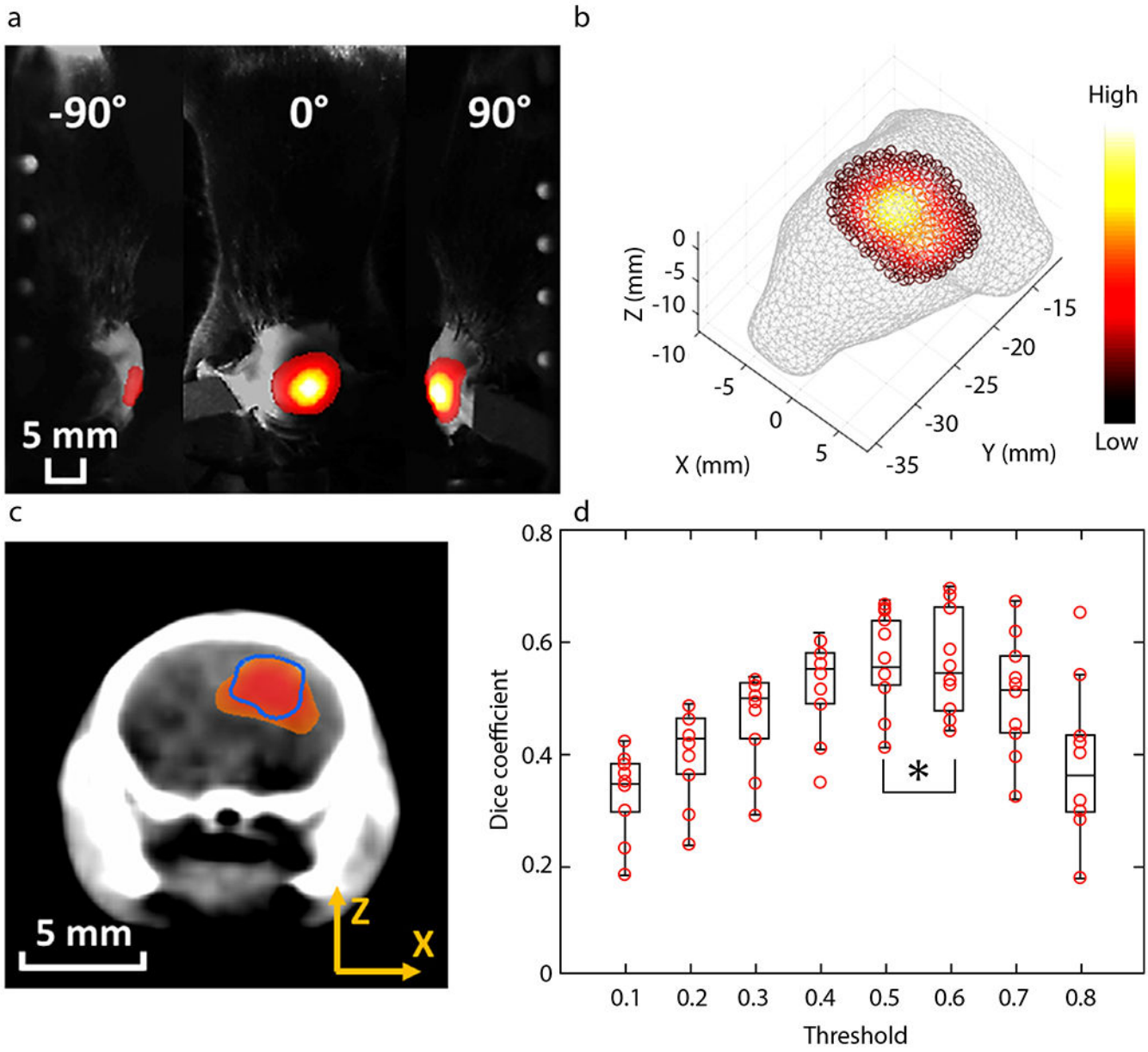

Fig. 3.

In vivo quantitative bioluminescence tomography (QBLT) reconstruction and threshold determination; (a) Bioluminescence imaging (630 nm; heat map) of a 2-week-old glioblastoma-bearing mouse taken at 3 projections. (b) The 3 projection bioluminescence images in (a) mapped onto the surface of the mouse head mesh. The mapped surface data larger than 10% of the maximum value among all the 3 projections is displayed in (a) and (b). (c) The overlap of GTV_{QBLT} (heat map, threshold at 0.5) and GTV (blue contour, contrast-labeled glioblastoma). (d) Dice coefficient between gross tumor volume (GTV) and GTV_{QBLT} versus threshold of maximum QBLT reconstructed value (n = 10); each red circle represents one mouse data point. The asterisk indicates no significant difference ($P > .05$) of Dice coefficient between the threshold of 0.5 and 0.6 groups.

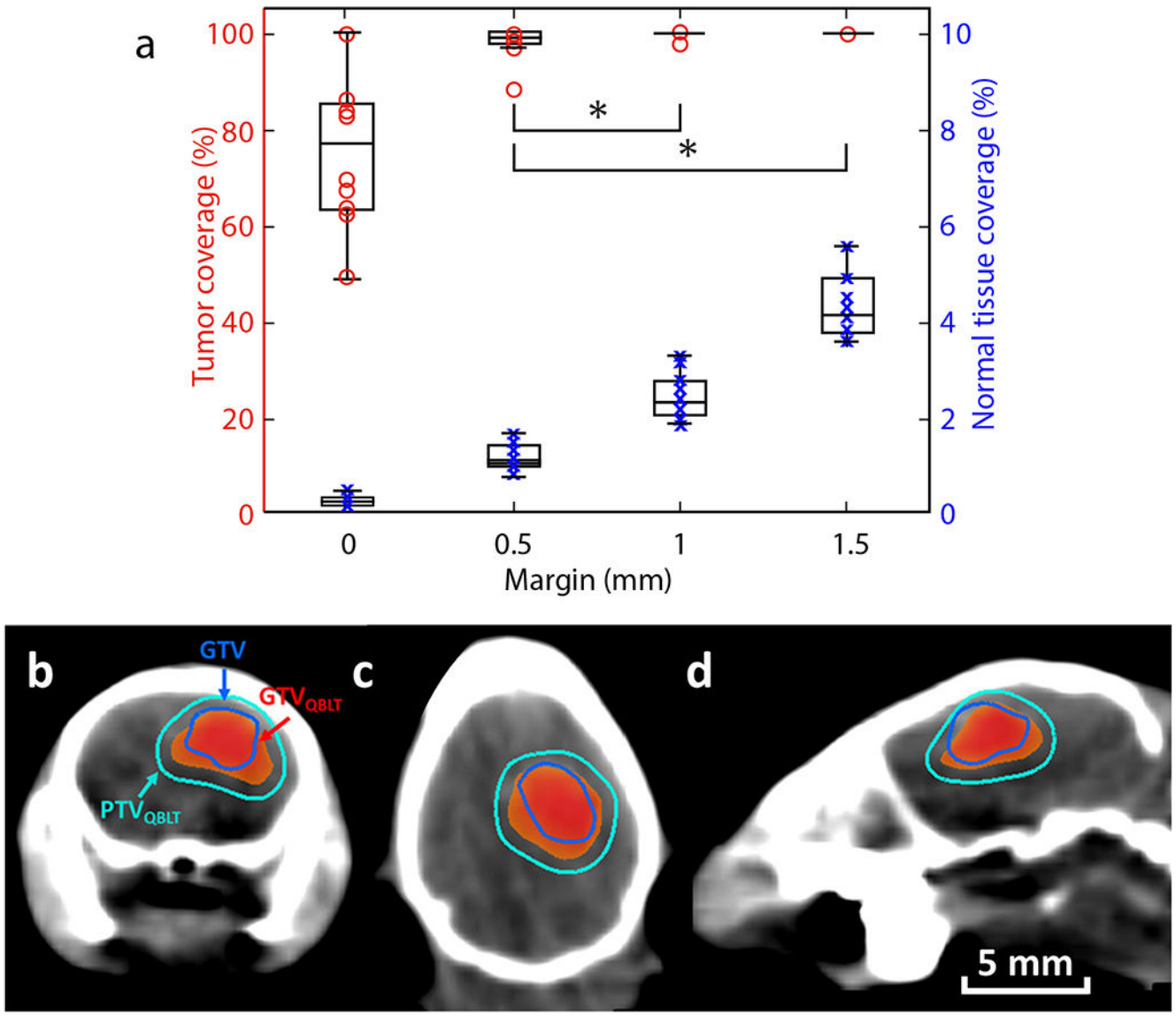

Fig. 4.

Margin design. (a) Tumor coverage (red circle, left axis) and normal tissue coverage (blue cross, right axis) versus margin expansion for 2-week-old glioblastoma. Asterisk indicates no significant difference ($P > .05$; n = 10) of the tumor coverage between the margin groups. Each circle and cross represent one mouse data point. (b-d) Representative case of a 0.5-mm margin added to a quantitative bioluminescence tomography reconstructed gross target volume (GTV_{QBLT}) (heat map) to form a PTV_{QBLT} (cyan). The blue contour is GTV (contrast-labeled glioblastoma). PTV = planning target volume.

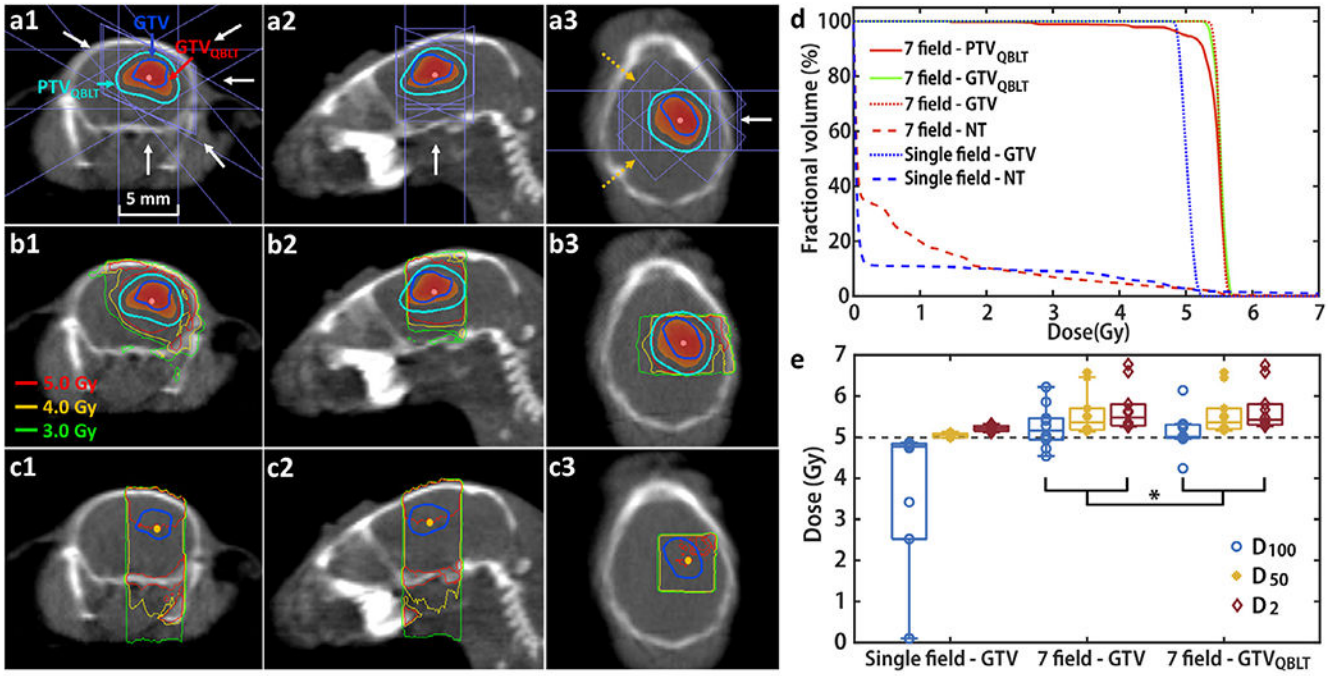

Fig. 5.

In vivo QBLT-guided conformal irradiation. (a1-a3) Representative case of a 7-field noncoplanar plan; the GTV is delineated in blue contour. Five coplanar fields (couch at 0 degree, and gantry at −60, 60, 90, 140, and 180 degrees) are indicated with white arrows, and 2 noncoplanar fields (couch at −40 and 40 degrees, gantry at −60 degrees) are indicated with the yellow dashed arrows. The weighting of each irradiation field is 12.5%, except for the beams at couch 0 degree and gantry 180 degrees with weighting of 25%. (b1-b3) Dose distributions for the 7-field plan (a1-a3), with 5 Gy as the prescribed dose to cover the QBLT planning target volume. (c1-c3) Dose distributions for single-beam delivery, with 5 Gy prescribed to the isocenter (yellow dot). (d) Dose-volume histogram of the 7-field QBLT-guided (b1-b3) and single-field (c1-c3) irradiation for PTV_{QBLT}, GTV_{QBLT}, GTV, and normal tissue. (e) Dose deposited at 100% (D_{100}), 50% (D_{50}), and 2% (D_2) of the target volume for GTV under the single field irradiation, GTV under the 7-field QBLT-guided irradiation, and GTV_{QBLT} under the 7-field QBLT-guided irradiation (n = 10). Black dashed line indicates the prescribed dose of 5 Gy. The asterisk indicates no significant difference ($P > .05$; n = 10) of D_{100}, D_{50}, and D_2 between the GTV and GTV_{QBLT} groups for the 7-field treatment plan. *Abbreviations:* GTV = gross tumor volume; NT = normal tissue; PTV = planning target volume; QBLT = quantitative bioluminescence tomography.

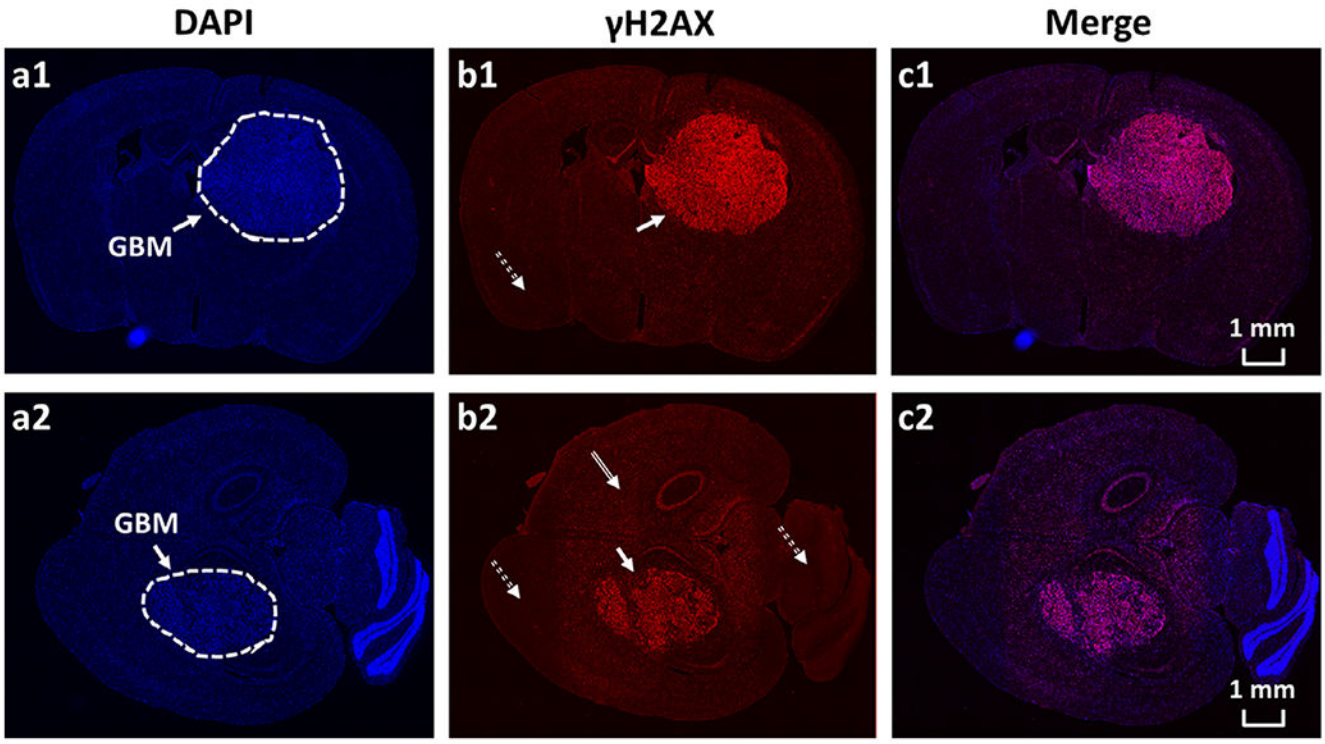

Fig. 6.

Pathologic confirmation of QBLT-guided conformal irradiation. (a1-b1, a2-b2) 4,6-diamino-2-phenylindole and γ-H2AX staining in transverse and coronal sections from 2 mice, respectively. (b1-b2) White solid, double dash, and double line arrows indicate the glioblastoma, normal tissue, and low-dose normal tissue irradiated area, respectively. (c1 and c2) Composite images. *Abbreviations:* DAPI = 4,6-diamino-2-phenylindole; GBM = glioblastoma; QBLT = quantitative bioluminescence tomography.